On the Topological Disparity Characterization of Square-Pixel Binary Image Data by a Labeled Bipartite Graph

Pablo Sanchez-Cuevas[1(✉)], Pedro Real[2], Fernando Díaz-del-Río[2], Helena Molina-Abril[3], and María José Moron-Fernández[1]

[1] Department of Computer Architecture and Technology, University of Seville, Seville, Spain
pablo-aries-7@hotmail.com, pabsancue@alum.us.es
[2] Research Institute of Computer Engineering (I3US), Sevilla, Spain
[3] Mathematical Institute of the University of Seville (IMUS), Sevilla, Spain

Abstract. Given an nD digital image I based on cubical n-xel, to fully characterize the degree of internal topological dissimilarity existing in I when using different adjacency relations (mainly, comparing $2n$ or $2^n - 1$ adjacency relations) is a relevant issue in current problems of digital image processing relative to shape detection or identification. In this paper, we design and implement a new self-dual representation for a binary 2D image I, called $\{4, 8\}$-region adjacency forest of I ($\{4, 8\}$-RAF, for short), that allows a thorough analysis of the differences between the topology of the 4-regions and that of the 8-regions of I. This model can be straightforwardly obtained from the classical region adjacency tree of I and its binary complement image I^c, by a suitable region label identification. With these two labeled rooted trees, it is possible: (a) to compute Euler number of the set of foreground (resp. background) pixels with regard to 4-adjacency or 8-adjacency; (b) to identify new local and global measures and descriptors of topological dissimilarity not only for one image but also between two or more images. The parallelization of the algorithms to extract and manipulate these structures is complete, thus producing efficient and unsophisticated codes with a theoretical computing time near the logarithm of the width plus the height of an image. Some toy examples serve to explain the representation and some experiments with gray real images shows the influence of the topological dissimilarity when detecting feature regions, like those returned by the MSER (maximally stable extremal regions) method.

Keywords: Hierarchical representation · Digital image · Topological dissimilarity · Parallelism · $(4 \cdot 8)$-adjacency tree · {4,8}-adjacency forest

1 Introduction

In 1979, Azriel Rosenfeld presented in [18] a new area of mathematical knowledge, called digital topology, that is dedicated to studying basic topological

properties of digital images. This work was later continued in [8]. Rosenfeld's framework uses a dual pair of adjacencies to get rid of connectivity paradoxes. This fact leads to ambiguities: depending on the chosen dual pair of adjacencies, the results may be different, even for the most elementary digital images processing algorithms. To overcome this problem, Latecki, Eckhardt and Rosenfeld [10] introduced in 1995 a new concept of $2D$ sets free from topological paradoxes, called *well-composed sets*. The connected components (CC, for short) of these sets (and of their complements) do not depend on the chosen connectivity. In others words, in the case of rectangular pixels, a set $D = I[1] \subset I$ is well-composed if and only if 8-adjacency (vertex-connectedness) implies 4-adjacency (edge-connectedness). It is clear that the two patterns consisting of four mutually 8-adjacent square pixels having four (Foreground or Background) 4-CCs are the only ones which are forbidden in well-composedness.

On the other hand, starting from a binary digital image I defined on a square grid, Rosenfeld [17] appropriately redefined the classical region adjacency tree representation of a continuous binary image (a tree-based representation of the nested relationship between the connected components in the image). Then the asymmetric concept of (a, b)-adjacency tree arose (a-adjacency for black/foreground/FG pixels and b-adjacency for white/background/BG pixel, such that $a, b \in \{4, 8\}$ with $a \neq b$).

In this paper, the problems of classification of 2D images in terms of degree of topological disparity or well-composedness and adjacency tree representations are both dealt with here. We use a complete parallel approach based on the HSF framework [14,15], allowing an efficient computation of all the needed structures and measures.

Section 2 contains a brief introduction to related works. In Sect. 3 some intuitive global topological discrepancy measures are defined. Section 4 explains the generation of the labeled bipartite graph $\{4, 8\}$-RAF, and in Sect. 5 the potential importance of local disparity measures derived from that representation in evaluating the topological robustness of the well-know feature detector MSER is uncovered. The paper concludes in Sect. 6.

2 Related Work

From a theoretical point of view, in this paper we propose a generalization of the classical topological Region Adjacency Tree (AdjT) notion to compute disparity-related properties. More concretely, these properties are based on the computing of topological Euler numbers and derived local and global homological information for adjacency graphs built with $(4, 8)$ and $(8, 4)$ adjacency pairs. The calculation of Euler numbers is well-known in literature, and several papers provide algorithms to make fast calculations on large images, as can be seen in [3,6,20], not only for 2D-images, but also for 3D-images [19]. Moreover, there exists a strong relation between these properties and the "well-composedness" problem in image analysis [1,2].

From a computational point of view, topology is the ideal mathematical scenario for promoting parallelism in a natural way, although it drives to less classical parallelism approaches. The nature of the topological properties is essentially qualitative and local-to-global, having the additional advantage that its magnitudes are robust under deformations, translations and rotations. Nevertheless, the results in the literature in that sense are rare. Up to now, the only topological invariant that has been calculated using a fully parallel computation is the Euler number [5]. Other authors have recently proposed parallel algorithms that compute some aspects of the homological properties of binary images [12]. In [16], a digital framework for parallel topological computation of 2D binary digital images based on a sub-pixel scenario was developed, modeling the image as a special abstract cell complex [9], in order to facilitate the generalization of this work to higher dimensional images. In addition, some software libraries of flexible C++ (RedHom, [13]) have appeared for the efficient computation of the homology of sets. These libraries implement algorithms based on geometric and algebraic reduction methods.

3 Topological Discrepancy of Binary Images Defined on a Square Grid

The topological duality properties of the (a, b)-adjacency tree are remarkable: (a) each a-connected component of the set $D = I[0]$ of FG pixels of I can be identified with exactly one 1-dimensional hole of its complement D^c; (b) and each b-connected component of the set D^c can be identified with exactly one 1-dimensional hole of D. Moreover, from an (a, b)-adjacency tree, we can straightforwardly extract an a-connected component labeling (CCL, for short) for D and a b-CCL for D^c.

Given the (a, b)-adjacency tree of I and in order to create a self-dual tool (that is, a model that coincides for I and for I^c), the first candidate is, without hesitation, the labeled forest formed by the two asymmetric adjacency trees $\{T_{(4,8)}(I), T_{(8,4)}(I)\}$ of I. Using as labeling set of FG (resp. BG) nodes in both trees the set of labels obtained in the 8-CCL of D (resp. of D^c), the resulting labeled forest, called $\{4, 8\}$-region adjacency forest ($\{4, 8\}$-$RAF(I)$, for short), will be the representation model from which intra and inter topological dissimilarity measures can be easily derived. It is immediate to see that the $\{4, 8\}$-$RAF(I)$ of I can be also described as a bipartite graph. Note that if I is a well-composed image, there is no internal topological dissimilarity. Due to the fact that in this case the $\{4, 8\}$-$RAF(I)$ is reduced to $T_{(4,8)}(I) = T_{(8,4)}(I)$, the local and global dissimilarity measures and descriptors of a non well-composed image must be constructed comparing invariants or topological features that are present in both trees. In this paper, we restrict our attention to global disparity characteristics.

Being I a non well-composed binary image and D the set of FG pixels of I, a first global topological discrepancy characteristic $dsm(\ )$ is based on the Euler number:

$$dsm(\aleph)(I) = |\aleph_8(D) - \aleph_4(D)| = |\aleph_8(D^c) - \aleph_4(D^c)|.$$

This is due to the fact that $\aleph_8(D \cup D^c) = \aleph_4(D \cup D^c)$ where $\aleph_a(C)$ $(a \in \{4,8\})$ is the classical Euler number of the set C of pixels, considering a-adjacency between them.

This heterogeneity number $dsm(\aleph)(I)$ can be obtained from the $\{4,8\}$-$RAF(I) = \{T_{(4,8)}(I), T_{(8,4)}(I)\}$ without difficulty. For instance, $\aleph_8(D)$ is the number of FG nodes in $T_{(8,4)}(I)$ minus the sum of the number of children of each FG node in $T_{(8,4)}(I)$. This is due to the fact that $\aleph_8(D)$ is globally defined in homological terms as the number of 8-CCs of D minus the number of 1-dimensional holes detected on the digital object D with 8-adjacency. An equivalent topological invariant of I to the "Euler" 4-dimensional vector: $(\aleph_8(D), \aleph_8(D^c), \aleph_4(D), \aleph_4(D^c))$ is the following one, called *Betti's vector of* I:

$$\beta(I) = (8CC(D), 8CC(D^c), 4CC(D), 4CC(D^c)).$$

where $a - CC(X)$ (resp. $a - HL(X)$) specify the number of $a - CC$s (resp. of 1-dimensional holes) the set of pixels X has $(a \in \{4,8\})$. Let us call *Betti's vector of* I to $\beta(I)$. This definition takes advantage of well-know homological duality properties between a-connected component and 1-dimensional b-holes ($a \neq b$ with $a, b \in \{4,8\}$).

Finally, given two binary images I and I' defined on a square grid, let us define the *global {4,8}-homological discrepancy* between I and I' as:

$$dsm(\beta)(I) = \sum_{i=1}^{4} |\beta(I)[i] - \beta(I')[i]|,$$

where $\beta(J)[k]$ means the k-component of the vector $\beta(J)$ $(k = 1, \ldots, 4)$ of the binary image J.

In the next section, the programming approach to compute the labeled forest $\{4,8\}$-RAF and derived local and global dissimilarity measures is shown.

4 Generation of the Bipartite Graph

In order to tackle the disparity between Adjacency Trees when employing $(4,8)$ and $(8,4)$-adjacency, a new hierarchical representation called $\{4,8\}$-$RAF(I)$ is developed here. This representation is computed by means of a bipartite graph. We consider the union of the $(4,8)$ and $(8,4)$-AdjTs and then add edges connecting two nodes of the same color FG or BG), one of each AdjT. That is, 4-CC nodes are connected to the 8-CC nodes containing them. In other words the $\{4,8\}$-$RAF(I)$ defines the inclusion relationships among regions from the AdjTs for both $(4,8)$ and $(8,4)$-adjacencies.

This computation is based on the algorithm $CCLT$ (Connected Component Labelling Tree) for labelling connected components published in [15]. An example of this (non-unique) $CCLT$ representation is shown in Fig. 1.

This $CCLT$ tree contains all the information related to the AdjT, having a unique root on the left bottom corner. This tree can be divided into rooted subtrees. Within each sub-tree, the root (called attractor) appears when an edge

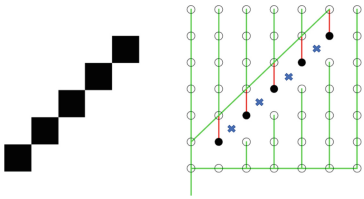

Fig. 1. Left: a synthetic image with 5 points in diagonal (using 4 adjacency criterion). Right: its double rooted tree. Blue crosses are added to represent the 8-connectivity of white pixels (crosses of the chessboard).

"touches" two different colors. This simplified representation implies a more efficient parallel topological computation [14,15]. From now on, the $CCLT$ will be the underlying topological encoding for all the digital image structures used in this paper.

In order to explain the consequences of the different adjacency criterion on our double rooted tree, Fig. 1, left, shows a simple but very common case when binarizing color images: the apparition of "thin" oblique lines. Using 8-adjacency criterion for FG pixels (and 4 for the BG ones) would evidently produce a single FG CC surrounded by the BG. But the reverse criterion drives to a very different composition (see Fig. 1, right): a set of 5 FG CCs of only one pixel each. Whereas BG pixels are really adjacent (blue crosses have been inserted to denote this adjacency) the tree for the BG regions "chose" the edge that runs parallel to the 5 FG pixels. Another tree building could have "decide" to cross among them, by inserting green edges along the blue crosses. These blue crosses represent alternatively the frontier between two FG regions. A fast measure of the disparity between these two adjacency criteria is computed from the Euler number. In the first case, this topological magnitude would value 1 for the FG pixels and $(1-1)=0$ for the BG ones. On the other hand, the opposite criterion (4-adjacency for the FG and 8 for the BG) would produce an Euler number of 5 for the FG pixels, and $(1-5)=-4$ for the BG ones (it has 5 holes, that are the FG pixels). Obviously, Euler number for the whole image remains to be 1 in both cases.

Figure 2 contains a synthetic image with a 4×4 chessboard that is surrounded by a monochrome background. The double rooted tree has been depicted with green edges for the tree connecting BG pixels and red edges ones for that connecting the FG ones. In addition, blue crosses have been inserted to represent the 8-connectivity of white pixels (crosses of the chessboard). These crosses represent the frontier among the FG components. The $(4,8)$-AdjT in this case is composed of a unique (8-connected) BG component that includes up to eight (4-connected) FG components. Note that the BG component is the root of the complete tree that ends in the left bottom pixel.

On the contrary, when using the opposite adjacency criterion, the very same image would have only two BG isolated 4-CC (marked with red numbers 1 and 2), and only one 8-adjacent FG region. The $(8,4)$-AdjT in this case would

be composed of an external BG component (previous background plus six BG pixels), containing the following nodes: a FG 8-CC, which includes, in turn, only the two internal remaining BG pixels 1 and 2. The Euler numbers would then be: $1 - 2 = -1$ for the FG region, and $3 - 1 = 2$ for the BG one.

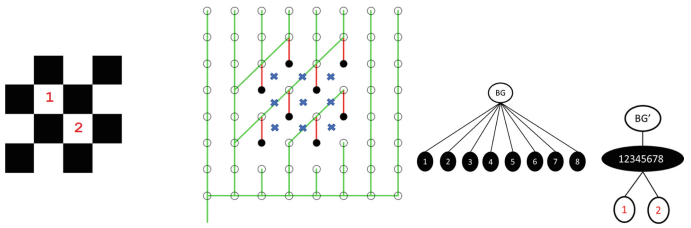

Fig. 2. Left: a synthetic image with a 4×4 chessboard surrounded by a monochrome background. Central left: its $CCLT$ for 8-connected BG (4-connected FG) –Green edges: BG tree; red edges: FG tree; blue crosses: the 8-connectivity of white pixels (crosses of the chessboard)–. Central right: $(4, 8)$-AdjT. Right: $(8, 4)$-AdjT.

Consequently, we propose an algorithm which firstly computes the $(4, 8)$ and $(8, 4)$-AdjTs and, then, adds the edges between pairs that follow the mentioned inclusion relationship. The complete pipeline is portrayed in Fig. 3.

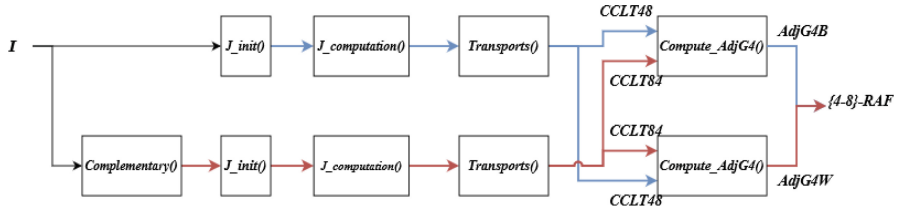

Fig. 3. Pipeline of the method for computing the final labeled bipartite graph $\{4-8\}$-RAF from an image I. $Compute\_AdjG4()$ function is defined in Fig. 7.

Indeed, the capability of the $CCLT$ to extract the topological information of the given image in the form of its AdjT in an efficient, parallel manner is here exploited. We can summarize the $CCLT$ algorithm in the following phases:

1. $J\_init()$: A jump matrix J of the same size as I is initialized, where each FG or BG pixel points into an 8-adjacent FG or a 4-adjacent BG pixel resp.
2. $J\_computation()$: Jumps/distances are propagated, where each pixel will eventually point into another of the same FG or BG region whose jump value is equal to zero. These pixels are provisional "attractors".
3. $Transports()$: Connectivity inconsistencies are solved, where the same region could be composed of different attractors. Hence, "false" attractors end up pointing into the "true" attractor of its FG or BG region.

Finally, $AdjT(I)$ has been implicitly defined in J once theses phases are performed, since the color-opposite region adjacent to each attractor is the region that surrounds the region of the attractor (which is a hole). Hence, this inclusion relationship builds up the AdjT of the image, with $(4, 8)$-adjacency.

Using this method, a straightforward solution for building the $(8, 4)$-AdjT of a given binary image I is as simple as computing the $(4, 8)$-AdjT of its complement I^c. This approach is feasible, by considering attractors as pixels not related to its color (FG or BG), using 8-adjacency for FG pixels and 4-adjacency for BG pixels. Thus, the relationship between attractors of both AdjTs is established.

Different 4-adjacent attractors of one AdjT are contained in the region represented by one 8-adjacent attractor of the opposite AdjT and, therefore, the bipartite graph $\{4-8\}$-RAF is formed. The proposed algorithm for such task is fully described in Fig. 7. Its execution consists of searching for 4-adjacent attractors (pixels with value equal to zero in the jump matrix J) via matrix scan and checking if that pixel is also an 8-adjacent attractor or, on the contrary, it has a jump value pointing into another 8-adjacent attractor. In the later case, a new edge in the bipartite graph is detected, and hence it is stored in a table containing all the 4 to 8-adjacency inclusion relations.

One example of the application of the proposed algorithm is shown in Fig. 4. Considering the original binary image and its complement, the results of computing the $CCLT$ algorithm are summarized in table of Fig. 5, where all the regions are stored with the linear indexes of their respective attractors. Finally, a bipartite graph is fully computed when checking the inclusion relations between attractors, and in this case the results are written as sets of 4-adjacent regions in parenthesis. Its graphical representation is portrayed in Fig. 6.

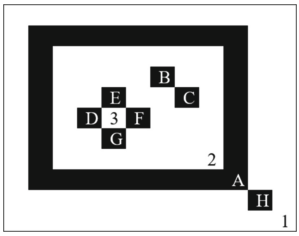

Fig. 4. A synthetic 11×12 binary image showing several cases where 4 and 8 adjacency criteria produce different adjacency trees. 4-regions are labelled with numbers and letters for BG and FG regions resp.

Once the $\{4, 8\}$-$RAF(I)$ is constructed, extracting local and global discrepancy measures (like $dsm(\aleph)(I)$ and $dsm(\beta)(I)$ defined in Sect. 3) is straightforward from $\{4, 8\}$-RAF (tables of Fig. 5). For the image in Fig. 2, the last two elements of $dms(\beta)$ are respectively the number of rows of each table; and the first two elements are computed as the number of labels that appear in the last column of each table, that is: $dsm(\beta)(I) = (3, 2, 8, 3)$.

	AdjG4W (from CCLT48)			AdjG4W
Column indexes:	0	1	**2**	3
Name of 4-white regions	Linear indexes of 4-white regions	Surrounding 8-black region	Surrounding 4-white region (of each 8-black region)	8-white region
1	131=11×12-1	(-)	(-)	131 (1)
2	92=7×12+8	105 (AH)	131 (1)	92 (23)
3	64=5×12+4	77 (DEFG)	92 (2)	92 (23)

	AdjG4B (from CCLT84)			AdjG4B
Column indexes:	0	1	**2**	3
Name of 4-black regions	Linear indexes of 4-black regions	Surrounding 8-white region	Surrounding 4-black region (of each 8-white region)	8-black region
A	105=8×12+9	131 (1)	(-)	105 (AH)
B	43=3×12+7	92 (23)	105 (A)	56 (BC)
C	56=4×12+8	92 (23)	105 (A)	56 (BC)
D	64=5×12+4	92 (23)	105 (A)	77 (DEFG)
E	53=4×12+5	92 (23)	105 (A)	77 (DEFG)
F	66=5×12+6	92 (23)	105 (A)	77 (DEFG)
G	77=6×12+5	92 (23)	105 (A)	77 (DEFG)
H	118=9×12+10	131 (1)	(-)	105 (AH)

Fig. 5. Tables containing the $\{4,8\}$-*RAF* (and CCL48 and CCL84 trees) of Fig. 4. The highest index of the 4-regions composing an 8-regions is considered to be an attractor for this image (which may fall elsewhere within the 8-region).

Moreover, our method allows to compute at the same time (without any additional time complexity) more information of the regions and contours, like areas and perimeters, which might be useful for further processing (see Sect. 6). Additionally, no processing step is done in a sequential manner. This allows to maintain the theoretical time complexity of the whole process near the logarithm of the width plus the height of the initial image.

5 $\{4,8\}$-*RAF* and Topological Feature Detectors

The $\{4,8\}$-*RAF* representation as well as the topological discrepancy measures proposed here are a fundamental tool for evaluating the robustness of image processing algorithms dealing with analytical or geometrical measures that strongly depend on the type of connectivity used for their calculation (area, perimeter, boundaries, curvatures, etc.).

In this Section, trying to illustrate this issue, we present a preliminary study about evaluating the robustness of the stability criteria used in the well known features detector algorithm MSER (Maximal Stable Extremal Region, [11]).

It is worth mentioning that the effectiveness of MSER for gray images is limited in its capability to detect regions of interest in extreme conditions, such as high contrast, low luminance, high light reflection, etc. [7]. Likewise, as the authors of [4] note, MSER is sensitive to blurring. Specifically, in blurred images, the values of intensity in the boundary of the regions change more slowly and this issue impact on the stability criteria on which the MSER is based. The limitations on blurred and/or textured images are related to image scaling, since blurring could be equivalent to image downscaling. Analogously, shapes

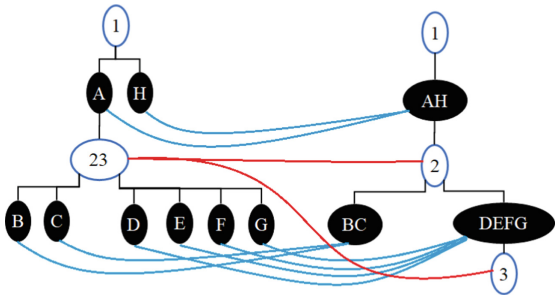

Fig. 6. (4, 8)-AdjT Right (Left) and (8, 4)-AdjT (Right) of Fig. 4. Relations between both trees (detailed in the tables of Fig. 5.) determine the Bipartite Graph.

associated with fine textures can vary fitfully in response to changes of scale. Specifically, the jutting fragments of non-convex MSERs are especially impacted by scaling changes [21]. It can be supposed that these issues could be related to the fact that the computing of the areas of the regions is carried out using 4-adjacency. Specifically, at [11], it is specified that the adjacency relation used is 4-adjacency. In fact, a small transformation that modifies the pixels diagonally, affecting connectivity at the 4-adjacency level, practically imperceptible in the image, causes an alteration in the number and location of the detected regions. The Figs. 8 and 9 illustrate this effect.

On the one hand, in Fig. 8 the MSER regions for the original image are shown using the *detectMSERFeatures()* MATLAB function. On the other hand, Fig. 9 shows the original image slightly modified to include additional 4-connected pixels by setting each horizontal couple with the same grey tone (that of the arithmetic mean of the values of both pixels). In addition the MSER regions for this modified image are also shown using the same MSER detector.

Note that both images are almost identical, but the ellipses that mark the area and orientation of regions have changed considerably. This is noticeable for the regions on the border of the most bottom coin: the slight change has introduced two new regions on the bottom, and other previous region on the left have disappeared. Likewise, a similar analysis can be discovered for the border regions of the most left coin.

Going further, the changes on the coin on the right of this last one are noticeable: instead of the seven original regions, the second image presents only four regions on this coin. The rest of coins have also suffered relevant changes on their MSER regions.

Additional tests have been done to slightly disturb the image by introducing 4 or 8 additional connected pixels. Specifically, it can be verified that the number of MSER regions change from the 60 of the original image to 51 for the previous Fig. 8, or 54 if the couple is done vertically. If 8-connected pixels were modified using the same arithmetic mean of two diagonal pixels, number of MSER regions would fall up to 47 for a left to right diagonal and 41 for the right to left one. Although the total number of detected MSER regions vary from 10 up to 32%,

Algorithm 1. [Building and relating Adjacent trees for both 4 and 8 adjacency criteria]

Input:
I: binary image of MxN pixels.
Output:
AdjG4B: CCLT Table for the 4-B regions/8-W regions and its correspondence with and 8-B regions
AdjG4W: CCLT Table for the 8-B regions/4-W regions and its correspondence with and 8-W regions

```
begin
//computing CCL trees of I and its complementary ! I
CCLT48 = CCL_tree (I); // 4 adj. for black pixels, and 8 adj. for white pixels,
CCLT84 = CCL_tree (! I);  // 8 adj. for black pixels, and 4 adj. for white pixels,

(n_4Black_regions , AdjG4B ) = compute_ AdjG4(CCLT48, CCLT84);
(n_4White_regions , AdjG4W ) = compute_ AdjG4(CCLT84, CCLT48);
end

function (idx_4, AdjG4) = compute_ AdjG4(CCLT1, CCLT2)
  idx_4 = 0; //index for the table of 4-black regions
  // matrixes CCLT48 and CCLT84 are indexed with a linear index running from 0 to M×N-1
  for l = 0: M×N-1 do
     // running along the CCL tree to extract the critical cells, that is, the representative of each region
     if (CCLT1 (l) == 0) then
        AdjG4 (idx_4)(0) = l;
        opp_idx = CCLT1 (l+1)  ;  // (l+1) points to a pixel of inverse color in the CCL_tree (I)
                                  // Only for the last pixel M×N-1 this indexation is not valid
        AdjG4 (idx_4)(1) = (l+opp_idx);
        idx8 = CCLT1 (l+opp_idx);
        AdjG4 (idx_4)(2) = idx8;

        // looking in the CCL_tree (!I) of the complement image
        idx8_2 = CCLT2 (l);
        AdjG4 (idx_4)(3) = (l+idx8_2); // this is the linear index of the 8 CC
        idx_4 = idx_4+1;
     end if
  end for
// finally idx_4 contains the number of 4-black regions,
// and the representative of the regions in the tables are ordered by the linear indexes
// theoretical time complexity is very near O(1) because the only loop-carried
// dependences among iterations is thus of the index idx_4 that fill the table.
```

Fig. 7. Algorithm 1. [Building and relating the $(4, 8)$ and $(8, 4)$-AdjT]

as previously mentioned, most regions (around 60%) change significantly from position, area or orientation, mainly those situated near the coin borders. Only those large evident regions, like that embedding a whole coin, are insensitive to these small changes.

It is worth to mention that this issue occurs in most gray images; we have simply chosen the coin examples because they clearly show the effect in the alteration of the MSER regions. This simple test illustrates the relevance of the

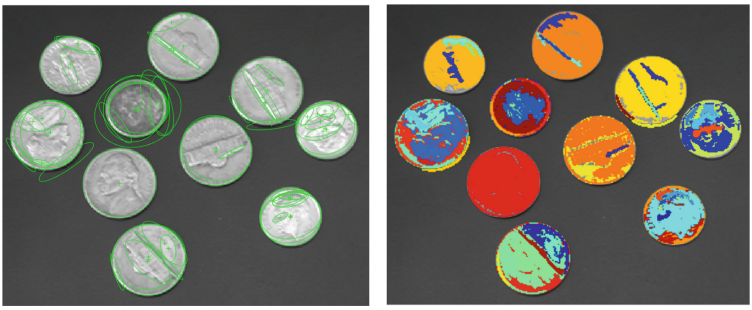

Fig. 8. Left: classical image of coins showing the MSER regions, with an ellipse that denotes their orientation and area. Right: same regions coloured.

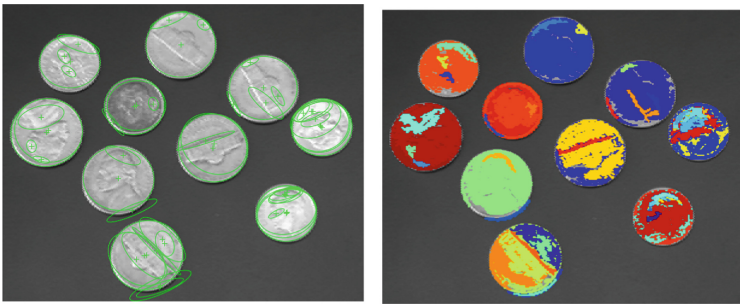

Fig. 9. Left: classical image of coins, slightly modified by adding additional 4-connected pixels, that includes the MSER regions, with an ellipse that denotes their orientation and area. Right: same regions coloured.

connectivity criterion when processing areas of images resulting from a threshold operation.

From this short analysis, the following starting hypothesis is plausible: Having at hand an efficient software for computing topological dissimilarity measures (like $dms(\beta)$) extracted from the $\{4,8\}$-RAF, constitutes a breakthrough in evaluating digital image processes that are based on the notion of topological region.

6 Conclusions

We propose here a parallel computational framework of a new hierarchical representation called $\{4,8\}$-RAF for digital images based on a square grid. As a conclusion from a basic analysis about the robustness of the stability criterion of the MSER feature detector, it can be said that an efficient software for computing (mainly, local) topological discrepancy measures derived from the RAF within the 2D and 3D context, could have a considerable influence on the fast and correct detection of characteristics in feature detectors that are based on the

topological notion of region. In a near future, we plan to advance in the following questions: (a) to have a fully operative software for calculating the $\{4,8\}$-RAF and derived local and global measures; (b) to design and implement a topologically improved MSER method; (c) to obtain the $\{4,8\}$-RAF (or, an equivalent graph structure) directly from the region contours via the Homological Spanning Forest model; and (d) to build a topologically robust computational framework of topological 3D disparity.

Acknowledgement. This study was funded by the research project of Ministerio de Economía, Industria y Competitividad, Gobierno de España (MINECO) and the Agencia Estatal de Investigación (AEI) of Spain, cofinanced by FEDER funds (EU): Par-HoT (Parallel Data Processing based on Homotopy Connectivity: Applications to Stereoscopic Vision and Biomedical Data, PID2019-110455GB-I00) and CIUCAP-HSF: US-1381077.

References

1. Boutry, N., González-Díaz, R., Jiménez, M., Paluzo-Hidalgo, E.: Strong euler well-composedness. J. Comb. Optim. (2021)
2. Boutry, N., Géraud, T., Najman, L.: A tutorial on well-composedness. J. Math. Imaging Vision **60** (2018)
3. Chao, Y., Kang, S., Yao, B., Zhao, X., He, L.: An efficient euler number computing algorithm. In: 2015 IEEE International Conference on Information and Automation (2015)
4. Chen, S.y., Cai, H., Wang, X., Xia, M., Wang, Y.: Entropy-based maximally stable extremal regions for robust feature detection. Math. Probl. Eng. **2012**, 857210 (2012)
5. Chiavetta, F., Di Gesù, V.: Parallel computation of the euler number via connectivity graph. Pattern Recogn. Lett. **14**(11), 849–859 (1993)
6. He, L., Chao, Y.: A very fast algorithm for simultaneously performing connected-component labeling and euler number computing. IEEE Trans. Image Process. **24**(9), 2725–2735 (2015)
7. Kang, S., Cha, D., Kim, Y., Han, D.: Text region extraction in high contrasting image. Int. J. Future Comput. Commun. **6**, 106–109 (2017)
8. Kong, T., Ronsenfeld, A.: Digital topology: introduction and survey. Comput. Vis. Graph. Image Process. **48**(3), 357–393 (1989)
9. Kovalevsky, V.: Algorithms in digital geometry based on cellular topology. In: Klette, R., Žunić, J. (eds.) IWCIA 2004. LNCS, vol. 3322, pp. 366–393. Springer, Heidelberg (2004). https://doi.org/10.1007/978-3-540-30503-3_27
10. Latecki, L., Eckhardt, U., Rosenfeld, A.: Well-composed sets. Comput. Vis. Image Underst. **61**(1), 70–83 (1995)
11. Matas, J., Chum, O., Urban, M., Pajdla, T.: Robust wide-baseline stereo from maximally stable extremal regions. Image Vis. Comput. **22**(10), 761–767 (2004)
12. Murty, A., Natarajan, V., Vadhiyar, S.: Efficient homology computations on multicore and manycore systems. In: 20th Annual International Conference on High Performance Computing, pp. 333–342 (2013)
13. REDHOM: http://redhom.ii.uj.edu.pl/. Institute of Computer Science, Jagiellonian University (2015)

14. Diaz-del Rio, F., et. al.: Computing the component-labeling and the adjacency tree of a binary digital image in near logarithmic-time. CTIC, pp. 82–95 (2019)
15. Diaz-del Rio, F., et. al.: Parallel connected-component-labeling based on homotopy trees. Pattern Recogn. Lett. **131**, 71–78 (2020)
16. Diaz-del Rio, F., Real, P., Onchis, D.: A parallel homological spanning forest framework for 2d topological image analysis. Pattern Recogn. Lett. **83**, 49–58 (2016)
17. Rosenfeld, A.: Adjacency in digital pictures. Inform. Control **26**, 24–33 (1974)
18. Rosenfeld, A.: Digital topology. Amer. Math. Monthly **86**, 621–630 (1979)
19. Toriwaki, J., Yonekura, T.: Euler number and connectivity indexes of a three dimensional digital picture. Forma **17**, 183–209 (2002)
20. Yao, B., He, L., Kang, S., Chao, Y., Zhao, X.: A novel bit-quad-based euler number computing algorithm. Springerplus **4**, 735–735 (2015)
21. Śluzek, A.: Improving performances of mser features in matching and retrieval tasks. In: Hua, G., Jégou, H. (eds.) ECCV 2016. LNCS, vol. 9915, pp. 759–770. Springer, Cham (2016). https://doi.org/10.1007/978-3-319-49409-8_63